Journal of the Brazilian Society of Mechanical Sciences and Engineering (2025) 47:175
https://doi.org/10.1007/s40430-025-05487-z

TECHNICAL PAPER

Fatigue life assessment of A356 aluminum alloy used for engine cylinder head

M. Angeloni[1] · C. O. T. R. Ruchert[1] · W. W. Bose Filho[1] · S. Pommier[2]

Received: 30 March 2023 / Accepted: 23 February 2025 / Published online: 17 March 2025

Abstract
This study investigates the fatigue resistance of cast A356 aluminum alloy used in engine cylinder heads, focusing on its behavior under high temperatures. Isothermal fatigue tests were performed at fixed temperatures of 120 °C and 280 °C, while in-phase thermo-mechanical fatigue tests spanned a temperature range from 120 to 280 °C. Fatigue crack growth rates were evaluated using different waveforms under displacement and load control conditions. Stress relaxation tests conducted from 75 to 280 °C provided essential data for modeling the material's mechanical properties. The results demonstrate that material heterogeneities and casting defects significantly impact fatigue performance, particularly at higher temperatures and under prolonged testing. The study highlights the role of porosity, which accelerates crack nucleation, reducing fatigue life by up to 50%. These findings offer valuable parameters for simulating fatigue behavior under cyclic thermal and mechanical loading, supporting the validation of Pommier and Risbet's crack propagation model. This research contributes to developing more durable engine components capable of withstanding extreme service conditions.

Keywords Cast aluminum · Thermo-mechanical fatigue · Fatigue crack growth · High temperature · Engine block

1 Introduction

Engine parts are routinely subjected to variations in temperature and load during service [1]. Exposure to high temperatures can lead to issues such as creep, oxidation (or corrosion), and fatigue, with these damage mechanisms acting independently or in combination, depending on factors like maximum and minimum temperatures, temperature range, mechanical strain, stress levels, strain rate (in-phase or out-of-phase), and environmental conditions [2–4]. High temperatures and mechanical loads facilitate crack nucleation and propagation, ultimately leading to fatigue failure, which may occur through high or low-cycle fatigue, either isothermally or anisothermally [5]. Therefore, understanding low-cycle fatigue resistance and the factors governing creep-fatigue interaction is essential for developing components capable of operating under extreme conditions.

Sehitoglu (1996) and Sarabanda (1991) demonstrated that components subjected to thermal cycling and mechanical loading undergo cyclic thermal creep (thermal ratcheting), a gradual accumulation of inelastic deformation after each cycle [1, 6]. This type of failure can result in ductile rupture, which may occur unexpectedly during service, especially when parts heat unevenly, creating localized deformations.

High porosity, particularly evident in the microstructure analysis (Fig. 3), significantly impairs the mechanical performance of cast aluminum alloys. The presence of porosities—up to 9.49% in the analyzed material—acts as stress concentrators, initiating cracks and reducing fatigue life by approximately 50%, as Buffière et al. (2001) reported. The observed porosity could be attributed to inadequate solidification during casting, leading to void formation. This defect has severe practical implications for engine components, especially cylinder heads, where thermal cycling and mechanical loads exacerbate crack propagation. To mitigate these effects, improving casting techniques and reducing porosity levels are crucial for enhancing the durability and reliability of such components [7, 8].

Technical Editor: Mario Eduardo Santos Martins.

✉ C. O. T. R. Ruchert
cassiusterra@usp.br

M. Angeloni
mauricio.angeloni@fatec.sp.gov.br

[1] Department of Materials, Engineering School of São Carlos, University of São Paulo, São Carlos, Brazil

[2] École Normale Supérieure de Cachan, Gif-Sur-Yvette, France

In combustion engines, cylinder head and valve temperatures rise rapidly during startup, while surrounding materials are cooled by water, which mitigates thermal expansion. This differential heating compresses the surface layers, generating compressive stresses. When cooling occurs, tensile stresses may develop. Thermal fatigue damage arises from these heating and cooling cycles, driven by temperature gradients that create internal stresses [1]. Additionally, mechanical strains caused by external loads, such as fuel explosions, exacerbate the situation, leading to thermo-mechanical fatigue, a combination of temperature variation and mechanical strain. This fatigue can trigger multiple damage mechanisms that alter the material's deformation behavior [9]. With repeated engine startups and shutdowns, the phenomenon is best understood as thermo-mechanical fatigue.

This study investigates the fatigue behavior of A356 aluminum alloy under both isothermal and in-phase thermo-mechanical fatigue conditions, focusing on the fatigue crack propagation rate as a function of temperature and waveform. Relaxation tests were also conducted to support the development of a computational model proposed by Pommier and Risbet (2005) for predicting fatigue crack growth rates at high temperatures [10–12].

2 Material and methods

2.1 Material

This study employed an aluminum–silicon alloy (A356) cast in a permanent mold by ASTM B108-08 (2008) from a cylinder engine head [13]. Its characteristics are good mechanical strength, high corrosion resistance, resistance to heat treatment, and good weldability [14, 15]. The chemical composition was analyzed using an optical spark emission spectrometer.

2.2 Methods

According to ASTM E3-11, the samples receiving the usual metallography preparation etched with Keller's reagent to assess the microstructure of α-phase size and morphology, eutectic phase distribution, and porosity using optical and scanning electron microscopes coupled to quantitative image analysis software [16, 17]. Figure 1a shows a specimen from the cylinder head to perform the mechanical tests; Figure 1b shows the specimens for tensile, isothermal fatigue, in-phase thermo-mechanical fatigue, relaxation, and fatigue crack propagation tests.

Figure 2 presents specimen size and geometry for tensile, relaxation, and fatigue tests.

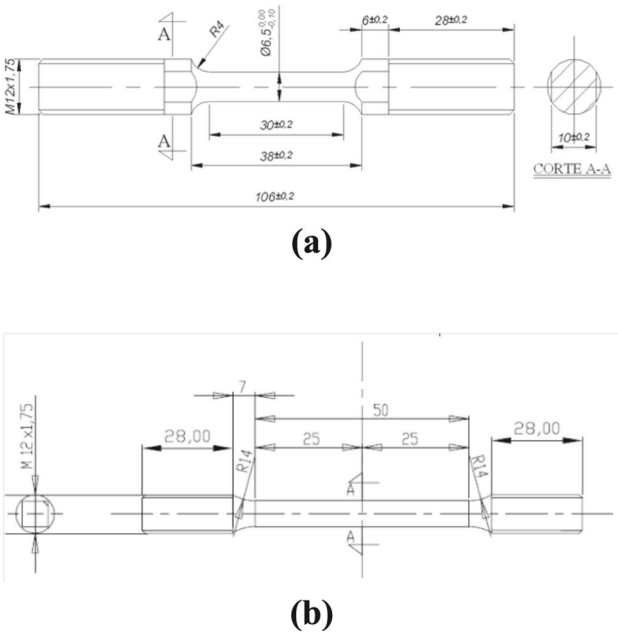

Fig. 2 Specimen size and geometry for **a** tensile, relaxation, isothermal fatigue, and in-phase thermo-mechanical fatigue tests and **b** fatigue crack propagation tests

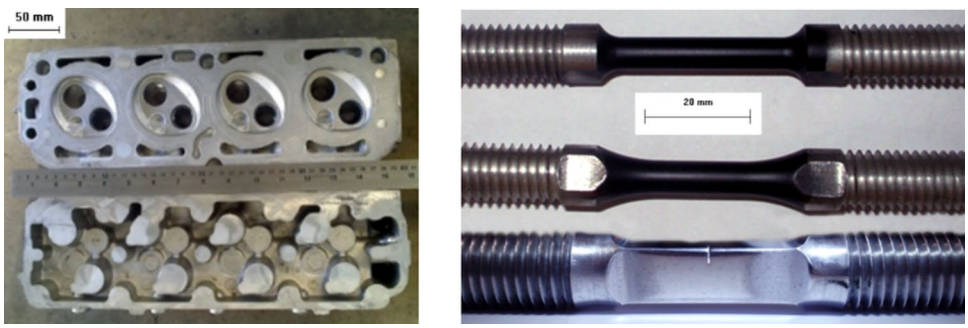

Fig. 1 **a** engine cylinder head from machined specimens and **b** machined, polished, and painted specimens

Tensile tests were conducted at room temperature, 120 °C, and 280 °C, according to ASTM E21-09 and ASTM E8/E8M-13, under displacement control at 0.003 mm/s [18, 19].

The testing for isothermal fatigue under controlled strain following ASTM E 606-12, 1 Hz frequency, mechanical deformation ratio $R_\varepsilon = -1$, and at two fixed temperatures: 120 °C and 280 °C (the starting and final temperatures of in-phase thermo-mechanical fatigue) [20]. The temperatures are because these values usually reach within engine cylinder heads. The failure criterion was a decrease in 50% of the maximum stress reached in the tests. Testing for in-phase thermo-mechanical fatigue was carried out according to ASTM E2368-10, from 120 to 280 °C, similar R_ε, and in relatively long periods (about 300 s), i.e., a lower frequency (0.003 Hz), which is quite different from that used for estimating isothermal fatigue because is difficulty in cooling down specimens while avoiding excessive temperature gradients [21]. Besides, testing for in-phase thermo-mechanical fatigue was conducted at a temperature range in a triangular waveform, with the highest temperature coinciding with maximum mechanical deformation and vice versa with both minimum values.

Corner notch-type specimens, shaped as per Pickard (1986), were tested for crack propagation at fixed temperatures (75 °C, 120 °C, 200 °C, and 280 °C) and loadings at stress ratio R = 0.1 obtained by a sinusoidal waveform and 10 Hz frequency [22]. A trapezoidal waveform, consisting of loading and unloading ramps of 10 s each and a 180 s dwell at maximum loading level, producing a total of 0.005 Hz frequency, was applied at the same temperatures—the monitoring of cracks occurred through EPD (electrical potential drop technique). Testing for stress relaxation was conducted in tensile at 80 °C, 100 °C, 120 °C, 140 °C, 180 °C, 240 °C, and 280 °C for total deformation levels of 0.1%, 0.3%, 0.5%, 0.7%, and 0.9%. The tests lasted 5 min, under strain control.

Scanning electron microscopy (SEM) was used to analyze the morphological aspects of fracture surfaces of some specimens tested for isothermal fatigue, in-phase thermo-mechanical fatigue, and crack propagation tests.

3 Results and discussion

3.1 Material

Table 1 compares chemical analysis results in nominal values found in ASTM A356 [23]. It also indicates that Fe and Cu amounts were slightly above nominal ones.

More significant amounts of iron and copper—the most common impurities in Al-Si alloys—may be detrimental to their mechanical properties since Cu weakens and Fe promotes the formation of acicular platelets in these alloys at high temperatures, which significantly reduce their ductility and fracture toughness. However, microstructural results in Fig. 3 indicate, as observed by Crepeau, 1998, the occurrence of a Chinese script-shaped phase, which is less detrimental to mechanical properties, due to iron forming this

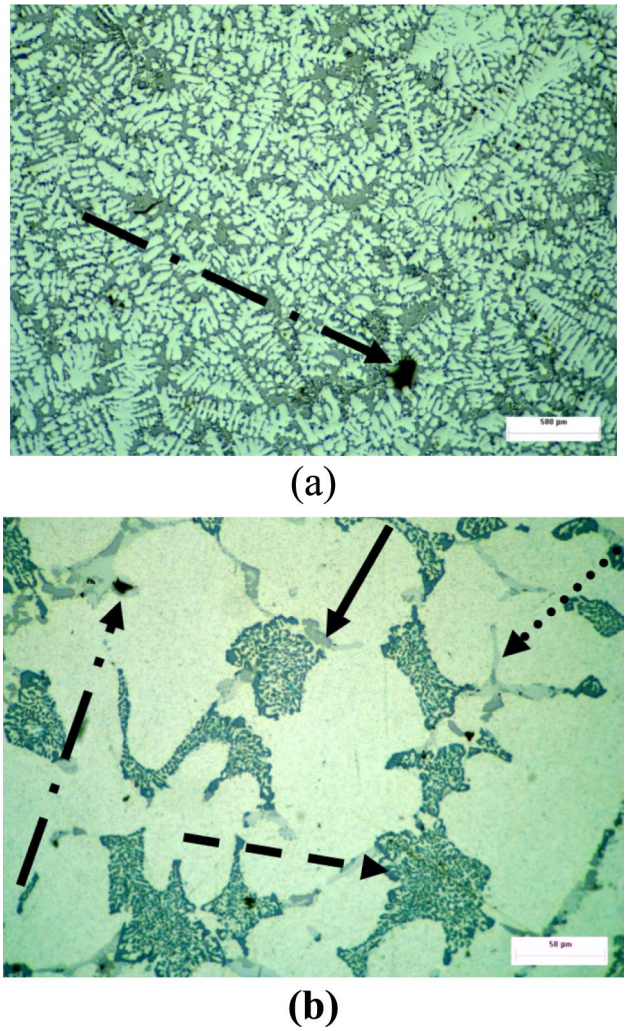

Fig. 3 Optical micrographs showing **a** well-defined dendrite microstructure and **b** coalesced silica particles that constitute the interdendrite eutectic (a dark gray area indicated by full arrow) and $Fe_2Si_2Al_9$-type precipitates (dotted arrow)

Table 1 Chemical analysis of A356 Al alloy (wt %)

Elements	Si	Mg	Fe	Cu	Zn	Mn	Ti	Al
Nominal	6.5–8.5	0.25–0.45	0.1–0.7	0.10–3.0	0.10–0.80	0.10–0.40	0.10_{max}	86.0–92.0
Actual	8.3	0.33	0.98	3.13	0.66	0.45	0.03	Base

more compact type of eutectic phase when balanced with manganese [24].

Chemical composition analysis was performed by energy-dispersive system (EDS) on fractured surfaces of specimens tested for fatigue crack propagation at different temperatures. It comprised the selection of 900 μm^2 sections of the crack propagation (CP) and final fracture (FF) regions. Results from this analysis show locally embrittled regions with high Cu and Fe concentrations (Table 2).

Figure 3 shows that the microstructure comprises primary α-phase, Si-rich eutectic phase, precipitates (Mg_2Si and Al_2Cu), and intermetallic components (Al_5FeSi, $Al_8Mg_3FeSi_6$, and $Al_5Mg_8Cu_2Si_6$). The microstructure is composed of well-defined dendrite structures with secondary dendrite arm spacing (SDAS) of approximately 25 µm, high porosity (Fig. 3a, b, dotted-dashed arrow), in addition to considerable change in silicon particles (Fig. 3b), full arrow). According to the ASM Handbook [17], the presence of $FeMg_3Si_6Al_8$-type (Chinese-writing type) (Fig. 3b, dashed arrow) and $Fe_2Si_2Al_9$-type (blade type) precipitates (Fig. 3b, dotted arrow).

Porosity was estimated using micrographs randomly taken in transversal and perpendicular directions under an optical microscope coupled to an image acquisition system. The material under analysis displayed an average porosity of 9.49% in area, with a typical porosity of 50 µm equivalent diameter. The study showed some voids with up to 500 µm equivalent diameter. These solidification voids act as stress concentrators and prematurely nucleate cracks inside or near the surface, thus decreasing or eliminating fatigue life for nucleation.

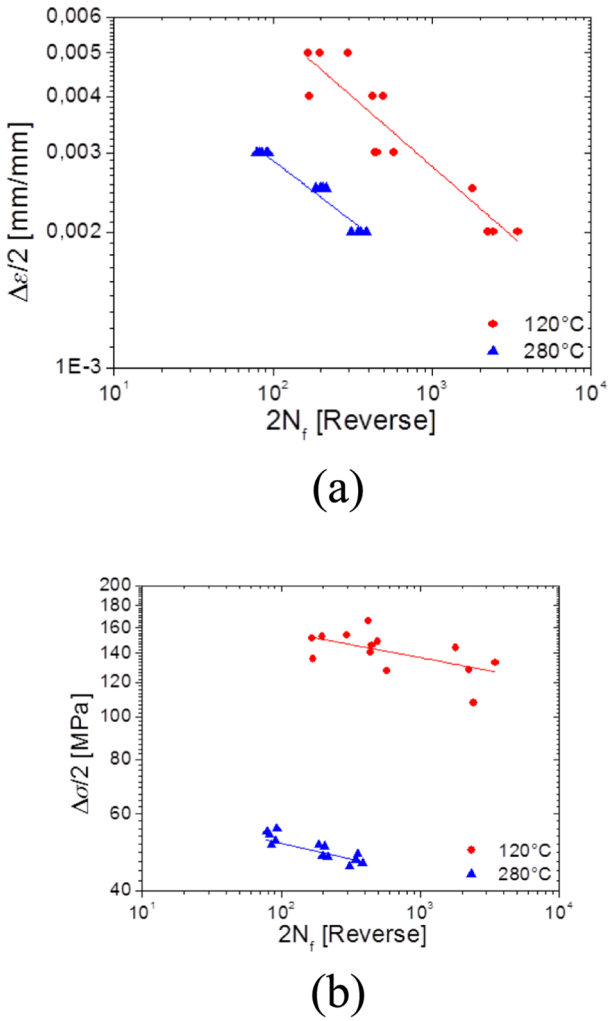

Fig. 4 **a** Strain amplitude versus several reversals to fail; **b** equivalent stress amplitude versus the number of reversals to fail (both tests at 120 °C and 280 °C)

3.2 Mechanical tests

Figure 4a illustrates the curve of strain amplitude versus several reversals to failure for isothermal fatigue tests at 120 °C and 280 °C (0.4 of the melting temperature), alongside the equivalent stress amplitude versus reversals to failure (Fig. 4b). A notable reduction in fatigue life was observed as the test temperature increased to 280 °C, aligning with findings by Suresh (1998), who attributed this behavior to mechanisms such as cyclic slip-induced cracks, grain boundary cavitation, and oxidation. Comparatively, studies by Buffière et al. (2001) on aluminum alloys confirm similar fatigue behavior under

Table 2 EDX (wt %) chemical analysis performed on the fracture surface

Test temperature (°C)	Region	Alloy elements					
		Al	Si	Mg	Mn	Fe	Cu
120	FF*	61.27	24.08	0.12	2.05	4.41	8.07
	CP**	69.72	29.23	0.33	0.03	0.01	1.4
200	FF*	67.41	6.80	1.66	0.18	0.29	23.67
	CP **	43.68	49.43	0.33	1.62	2.26	3.34
280	FF*	48.47	19.02	0.14	1.61	4.91	25.85
	CP**	77.37	9.88	0.93	0.10	0.13	11.59

*Final fracture; **Crack propagation

high-temperature conditions, emphasizing the role of microstructural degradation in reducing fatigue life. [25].

Figure 5 shows stress versus plastic deformation hysteresis curves obtained from isothermal fatigue data at 120 °C and 280 °C for 0.3% total mechanical deformation. These curves observe two distinct behaviors: A356 hardens cyclically at 120 °C and softens cyclically at 280 °C. As is well-known, high temperatures promote atom rearrangement in crystal structures, i.e., atoms shift around to reach a better and less faulty arrangement, thus facilitating the movement of dislocations.

It is also noteworthy that under tensile and compression loadings at both 120 °C and 280 °C, A356 displays distinct behaviors in terms of stress magnitude. This difference in mechanical behavior is more marked at lower temperatures. At higher temperatures, this difference is subtler as dynamic microstructural recovery is favored, which promptly decreases the density of dislocations, and the material is allowed to deform without further increase in stress plastically. Porosity, nearly 10% in this material, may have contributed to the difference observed since it anchors dislocations.

Figure 6 shows results from in-phase thermo-mechanical fatigue tests at temperatures ranging from 120 to 280 °C. Also, it generates isothermal fatigue test results on the same graph for comparison. Sehitoglu (1996) observed that, in general, isothermal tests could not adequately represent thermo-mechanical fatigue behavior (TMF). An exception exists when the cost and time required to conduct TMF tests are considered [1]. Along these lines, it is observed that A356 life is quite similar to that obtained for isothermal fatigue at 280 °C when tested for in-phase thermo-mechanical fatigue. Besides, it may be inferred that significant damage when testing for in-phase thermo-mechanical fatigue almost exclusively occurred at maximum temperature.

This frequency can be considered too high despite testing for isothermal fatigue at a lower frequency (0.1 Hz) compared to that employed to estimate in-phase thermo-mechanical fatigue (0.003 Hz). Therefore, during in-phase thermo-mechanical fatigue tests, exposition time at higher temperatures gives rise to another phenomenon known as relaxation, which explains the difference between the hysteresis loops obtained for isothermal fatigue and in-phase thermo-mechanical fatigue, as shown by stress–strain behavior in Fig. 7. This phenomenon interacts with fatigue due to extended testing periods and the fact that testing is under strain control. Hence, even though fatigue life is quite similar and may be used to estimate in-phase thermo-mechanical fatigue life for this Al alloy, this difference is significant and must consider the relaxation in fatigue life simulation.

To identify viscous behavior in the in-phase thermo-mechanical fatigue tests shown in Fig. 7, stress relaxation was measured at fixed temperatures of 80 °C, 100 °C,

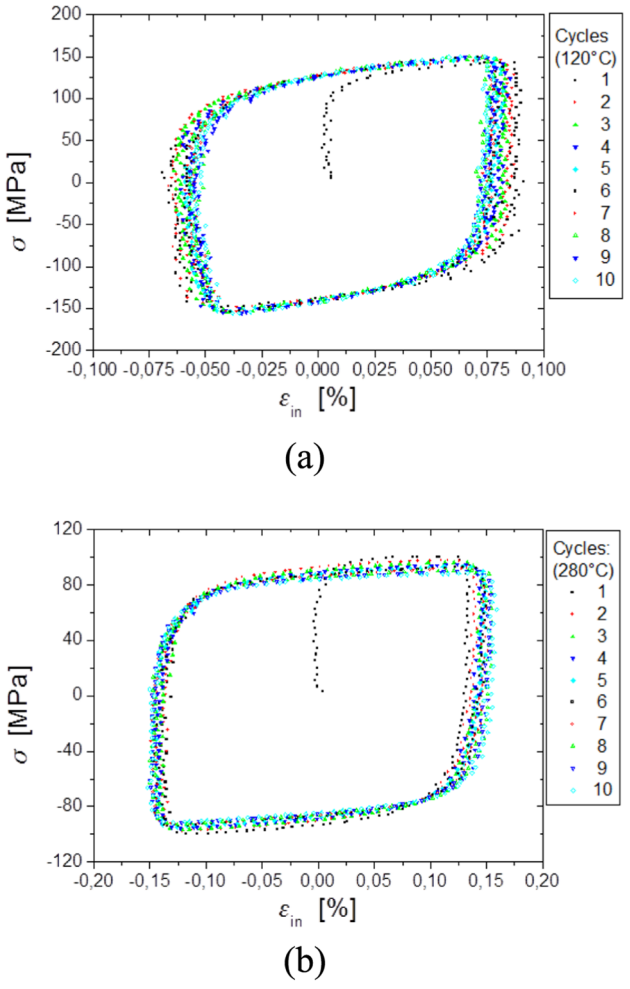

Fig. 5 Isothermal fatigue tests. Hysteresis curves for total mechanical deformation of 0.3% at **a** 120 °C and **b** 280 °C

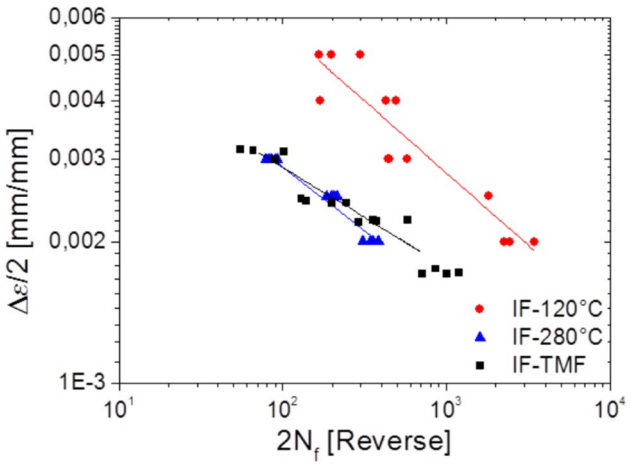

Fig. 6 Total mechanical strain amplitude versus several reversals to failure for isothermal fatigue and in-phase thermo-mechanical fatigue tests

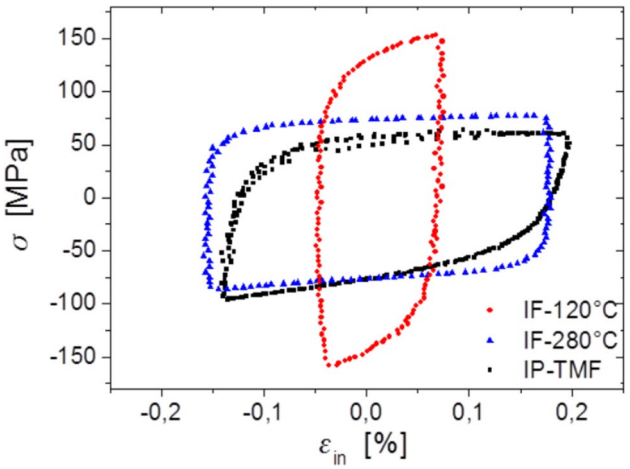

Fig. 7 Hysteresis related to isothermal and anisothermal tests for 0.3% total mechanical deformation

120 °C, 140 °C, 180 °C, 240 °C, and 280 °C, for total deformation levels of 0.1%, 0.3%, 0.5%, 0.7%, and 0.9%, and under five-minute dwell. Testing was performed under strain control with trapezoidal waveform using a special extensometer to measure strain at high temperatures. Figure 8 shows results for 100 °C and 280 °C. Similar to the hysteresis from isothermal fatigue tests, the hysteresis obtained for relaxation tests indicates two distinct behaviors, with 240 °C being the threshold temperature. A356 hardens cyclically at lower temperatures while softening cyclically at higher temperatures. High temperatures promote atom rearrangement within the crystal structure, i.e., atoms shift positions to reach a better and less faulty arrangement. This facilitates dislocations, causing the material to soften.

Load versus elastic and plastic deformation curves are shown in Fig. 9, which also indicate that when testing under controlled strain, i.e., the total strain was kept constant throughout the test, there was an increase in plastic deformation and, consequently, a decrease in elastic deformation, so that the total deformation remained constant. Therefore, this increase in plastic deformation corresponded to creep deformation. Under 5-min dwell time and at 0.5% total strain, plastic deformation increased, and as a result, the load necessary to keep total strain constant decreased. Therefore, given that specimens remain at high temperatures for a long time because of the meager strain rate in in-phase thermo-mechanical fatigue tests, the influence of creep is quite strong.

Notwithstanding, despite their significant size, as shown in Fig. 3, solidification voids can hardly be detected through conventional techniques, such as ultrasound and X-ray, employed regularly at the production line, especially on specimens used for microstructure analysis. More importantly, the observations made on the fracture surface of specimens tested for isothermal fatigue under TMF conditions indicated that solidification voids quickly nucleated cracks in the component under cyclic loading conditions.

Therefore, the component life was based on crack propagation life and the execution of testing on specimens

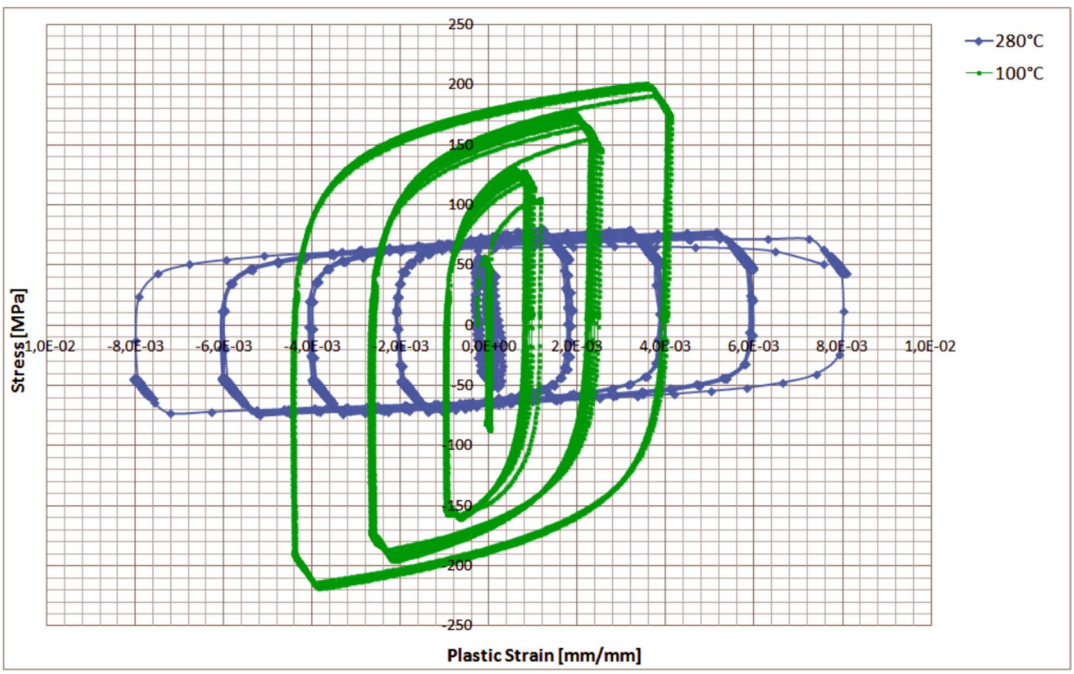

Fig. 8 Relaxation test hysteresis for total deformations of 0.1%, 0.3%, 0.5%, 0.7%, and 0.9% at 100 °C and 280 °C

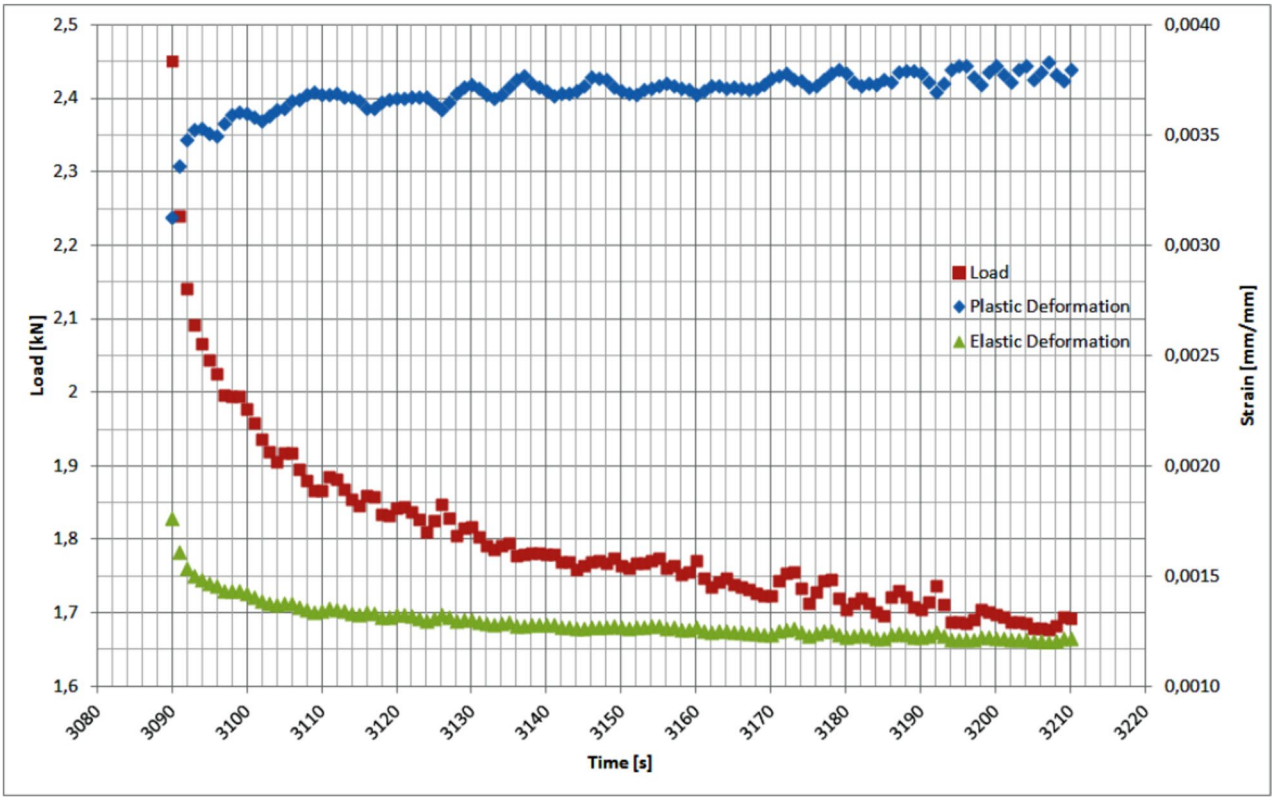

Fig. 9 Load versus elastic and plastic deformation under a total strain of 0.5% at 280 °C under five-minute dwell

deriving from a cylinder head. This fact limited the size of specimens, which were machined to feature a unique geometry, as shown in Fig. 2. The temperature for the tests was 75 °C, 120 °C, 200 °C, and 280 °C, and loading ratio of R = 0.1, 10 Hz frequency, and under two different loading conditions: (a) sinusoidal waveform and (b) trapezoidal waveform (dwell), the latter consisting of loading and unloading ramps lasting 10 s each and a 3 min dwell at constant load (dwell-L) and under displacement control (dwell-d) at approximately 0.005 Hz. The evaluation of the crack growth according to ASTM E1457/13 by potential drop methodology was used for [26].

Figure 10 shows the results from crack propagation tests. Regarding fatigue tests under sinusoidal waveform and load control, for the same ΔK, as the test temperature increased, the fatigue crack growth rate gradually increased because of decreasing mechanical strength, as generally reported in the literature. The results showed a general tendency for increased data spread as temperature rises, which can be attributed to the influence of temperature on the material microstructure, exacerbating its flaws, for example, porosity and lack of chemical homogeneity, that impact its local mechanical strength. As to the dwell type cycle, for the same temperature, it is possible to note that dwell loadings are comparatively more detrimental since they give rise to creep, which interacts with mechanical fatigue, causing crack growth rates to change significantly. Still, considering the fatigue crack propagation at 280 °C under load and displacement control, a very different fatigue behavior is found. In the case of displacement control, stress relaxation takes place at the crack front, ΔK decreases rapidly, and as a result, the crack propagation rate is nearly constant.

Figure 11 shows displacement measurements over time during tests for fatigue crack growth rate at 120 °C and 280 °C under dwell cycles and controlled load. For a constant initial load and similar initial crack size, displacement at 280 °C was significantly higher during tests, thereby indicating accumulation of creep deformation over time. This phenomenon interacts during long plateau periods, causing the material to "flow." Thus, cracks propagate due to the interaction between fatigue and creep, i.e., not only due to fatigue, but also sinusoidal wave loading. Creep may influence crack initiation and growth because creep damage is caused by cavity nucleation on grain boundaries because of coalescing voids, stacking dislocations, and sliding grain boundaries. The same can happen to second-phase particles. Subsequent growth of these cavities is conducive to grain boundary cracking and intergranular fracture. Under static loading, failure occurs using catastrophic fracture when cavities coalesce.

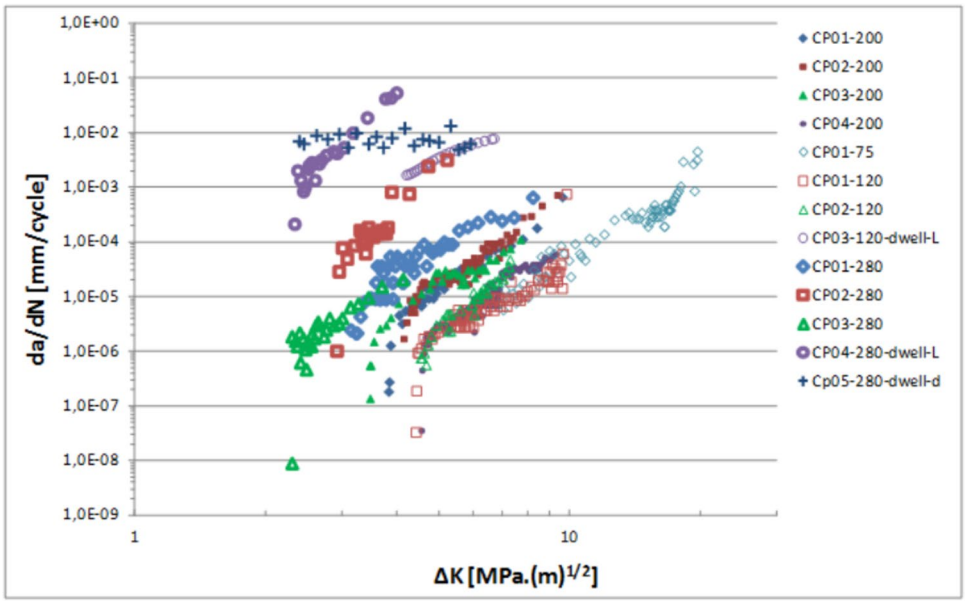

Fig. 10 Crack propagation rate (**da/dN**) as a function of stress intensity factor variation (**DK**) at 75 °C, 120 °C, 200 °C, and 280 °C and under a sinusoidal wave and dwell loadings

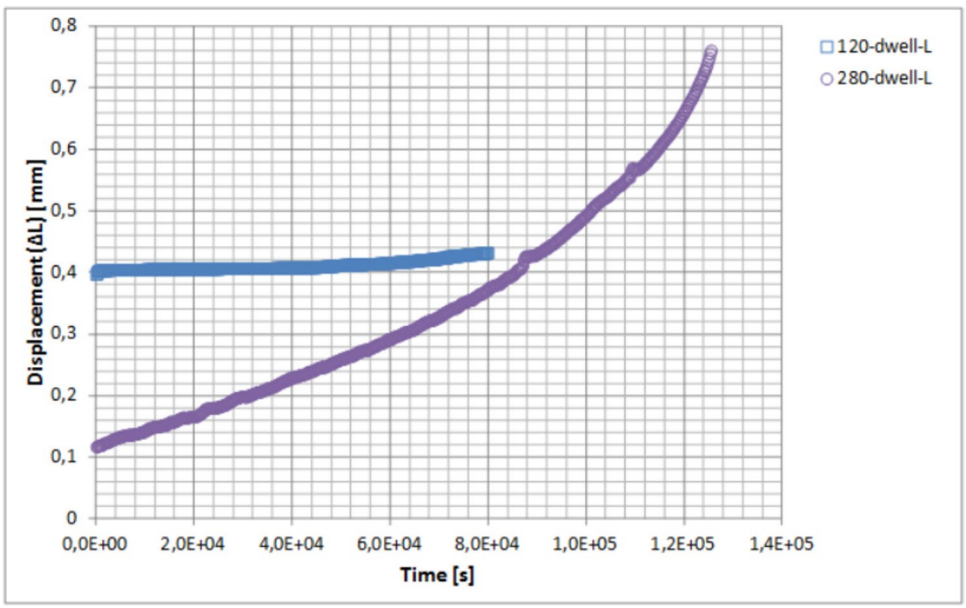

Fig. 11 Displacement versus time curves for a crack propagation test under dwell loading

Fracture surface analyses were performed using a scanning electron microscope (SEM) in conjunction with the deformation map for Al presented by Roesler et al. (2007) to guide the discussion [27]. Figure 12 presents SEM fractography from the stable crack growth region at 120 °C under sinusoidal (Fig. 12a) and dwell (Fig. 12b) cycles. In both cases, mechanical fatigue constituted the micromechanism, with the precise formation of striations, as shown in Fig. 12d. At 200 °C (Fig. 12c), the identification of fatigue striations on the fracture surface (Fig. 12d) since at higher temperatures, A356 displayed higher ductility than at 120 °C. The fatigue cracks growth rate for similar DK was higher than that at 120 °C. However, in light of the deformation mechanism map presented by Roesler et al. (2007), for this temperature, two micro-mechanisms may cause plastic deformation: dislocation glide and dislocation creep [27]. Under low external stress and at low temperatures, the material deforms elastically.

Similar to deformation at low temperatures, creep deformation can also occur by metal dislocation. Nevertheless, there is one crucial difference: if a dislocation edge encounters an obstacle, for example, a precipitate, it will need a minimum stress value to overcome the obstacle at low temperatures. On the other hand, if a dislocation edge encounters an obstacle at higher temperatures, the dislocation can evade the obstacle by adding or emitting vacancies, thereby

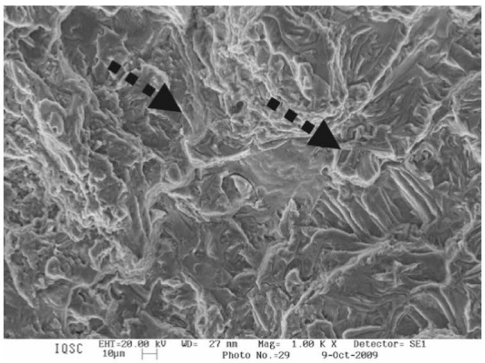

(a)

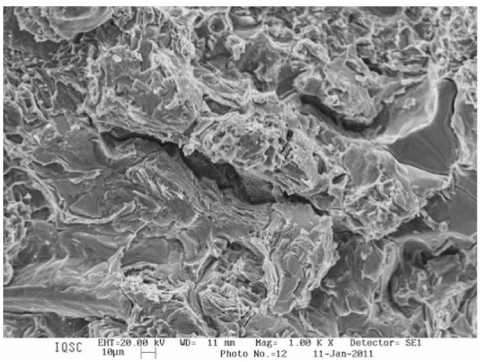

(b)

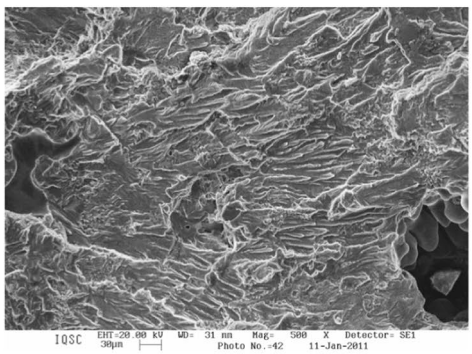

(c)

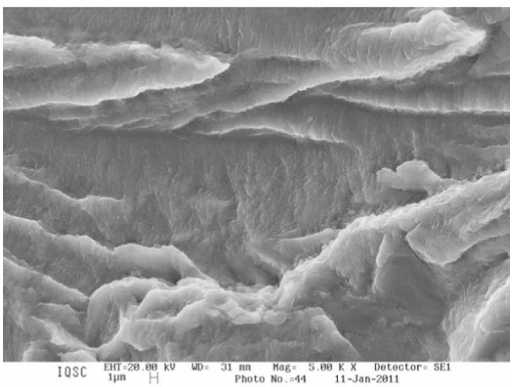

(d)

Fig. 12 **a** General aspect of fracture surface from a specimen tested for fatigue at 120 °C, **a** sinusoidal and **b** dwell cycles under load control; **c** fracture surface of a specimen tested for fatigue at 200 °C, under load control and sinusoidal waveform; **d** detail of (**c**)

escaping its original slip plane. Diffusion creep starts at higher temperatures, being stronger under low stress than under dislocation creep because of its lower creep exponent. Due to the lower activation energy needed for grain boundary diffusion, this mechanism overrides bulk diffusion at low temperatures. Since the creep exponent is the same in both cases, the two regions are separated by a vertical line.

Figure 13 shows the fracture surface of a specimen tested for fatigue at 280 °C under dwell cycles and load control. Crack propagation was mainly due to creep, with dimples appearing extensively at the crack front during dwell. Since a crack starts propagating at a relatively low ΔK, diffusion creep may have occurred in this case. As the crack grows, ΔK rises, and crack growth quickly accelerates.

Figure 14 shows the fracture surface of a specimen tested for fatigue at 280 °C and under dwell cycles and displacement control. This surface indicates a fatigue micromechanism of fracture similar to that under load control. However, stress relaxation occurs at the crack front in this case, and ΔK decreases rapidly while the crack propagation rate remains nearly constant. The fracture surface shows a mixture of dimples (creep) and mechanical fatigue features [28, 29].

Finally, to better contextualize the contributions of this study, it is essential to compare the experimental results obtained with those of previous works. The chemical composition analysis of the materials revealed that the concentrations of Fe and Cu were slightly above the nominal values specified by ASTM A356, corroborating the observation that impurities such as Cu and Fe can be detrimental to the mechanical properties of Al-Si alloys, as reported by Suresh (1998) and Buffière et al. (2001). These authors emphasized that high levels of Cu can weaken the material matrix and that the presence of Fe may promote the formation of acicular precipitates, thereby reducing ductility and fracture toughness.

On the other hand, the microstructural results indicated the formation of a eutectic phase with less detrimental characteristics, aligning with the research by Crepeau (1998), which observed that the Chinese script-shaped phase is more compact and can enhance mechanical properties when balanced with manganese. This divergence between chemical composition and microstructural results is crucial, as it suggests that, although impurities may reduce mechanical strength, their interaction with the microstructure can mitigate some of these adverse effects.

Furthermore, the fatigue tests conducted in this study revealed a behavioral pattern consistent with existing

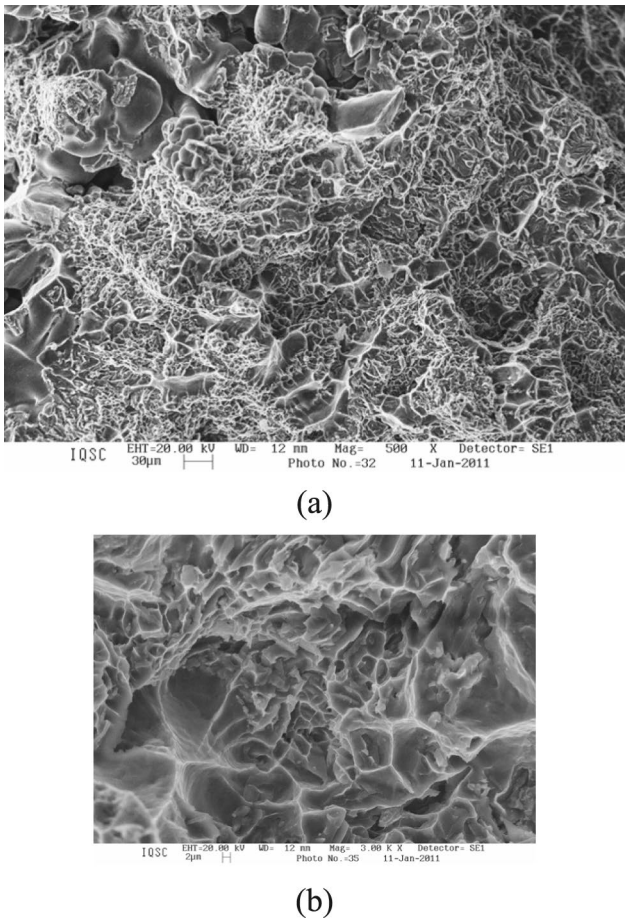

Fig. 13 General aspect of the fracture surface of a specimen tested for fatigue at 280 °C, under dwell cycle, and load control: **a** stable crack growth region and **b** detail of (**a**)

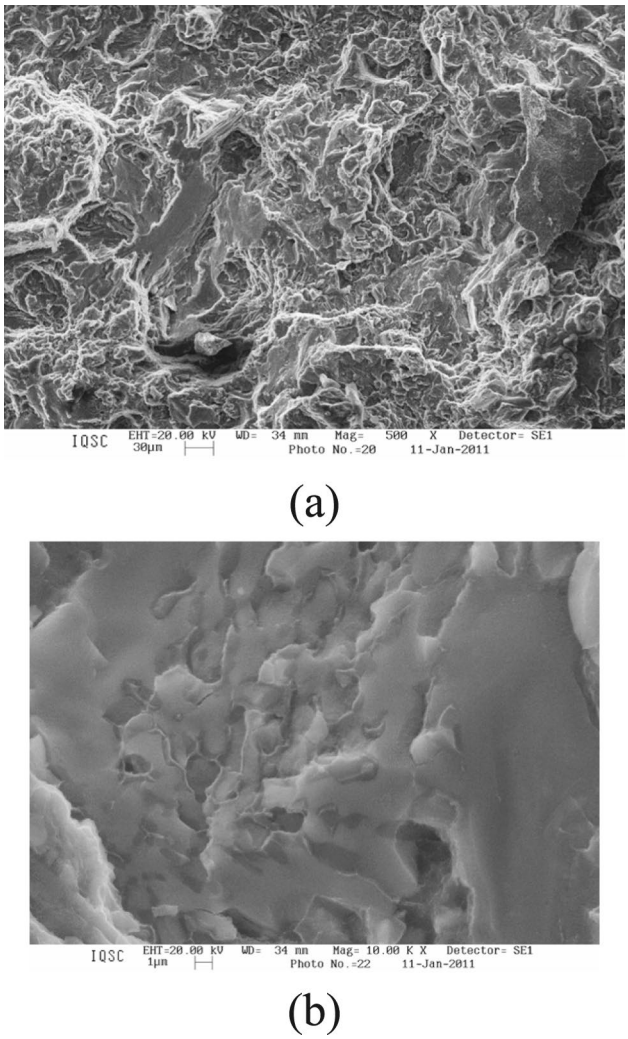

Fig. 14 SEM analysis from a specimen tested for fatigue at 280 °C, under dwell cycle and displacement control: **a** region of stable crack growth and **b** detail of (**a**)

literature. The reduction in the material's lifespan with increasing temperature, as observed in the isothermal tests, aligns with the findings of Suresh (1998) and Buffière et al. (2001), who also documented microstructural degradation under high-temperature conditions. However, the present study advances the understanding of the interaction between fatigue and creep, demonstrating that under displacement loading conditions, crack growth behaves differently, exhibiting an almost constant crack propagation rate due to stress relaxation. This aspect has not been extensively explored in prior research.

4 Conclusions

The die-cast A356 Al alloy displayed a microstructure with relatively coarse dendrites in a eutectic matrix, a mean SDAS of 25 µm, intermetallic precipitates, and porosities with a mean diameter size of 50 µm and a maximum size of 500 µm.

Considering the isothermal fatigue tests under strain control, as the temperature rose from 120 to 280 °C, life was reduced because A356 became less resistant to plastic deformation and had an increasing number of defects. The stabilized hysteresis loop indicated a difference in ductility, as well as the fact that during testing at 120 °C, the material in question cyclically hardened while cyclically softening at 280 °C.

In-phase thermo-mechanical test, results indicated that the fatigue life of A356 is quite similar to that obtained from isothermal tests at 280 °C and that the most severe damage occurred at the highest temperature. Also, both hystereses are pretty similar in shape, with some disparities since the thermo-mechanical cycle is slower (0.003 Hz) than the isothermal one (0.1 Hz), which allows stress relaxation to occur, thereby reducing the maximum stress level.

Relaxation tests indicated two distinct behaviors, 240 °C being the threshold temperature. At lower temperatures, A356 hardens cyclically while softening cyclically at higher temperatures. This behavior is similar to that observed during tests for isothermal fatigue. Since the tests were carried out under strain control, stress relaxation is present during dwell, reducing the elastic component of strain while concurrently increasing its plastic component. The higher the test temperature, the lower the amount of stress.

Results for fatigue crack growth show that temperature and waveform substantially impact both crack growth rate and stress intensity threshold. About the sinusoidal waveform (10 Hz), when the temperature increased, ΔKth decreased, and the crack propagation rate increased (for a constant K). However, the change in the crack propagation rate by fatigue (da/dN) with temperature is quite similar, indicating that the crack growth micro-mechanism does not change because of the high frequency used; it was due only to loss of mechanical strength instead.

For stress-controlled testing at constant temperatures (120 and 280 °C), when the waveform changed from sinusoidal to 3-min dwell at maximum load, the crack propagation rate increased by approximately 100 times, indicating a significant contribution from creep to crack propagation. The amount of creep contribution is dependent on temperature; i.e., the higher the temperature, the more significant the contribution from creep.

In strain-controlled testing at constant temperature (280 °C) and under 3-min dwell at maximum load, the crack propagation rate (da/dN) as a function of ΔK became nearly constant because of stress relaxation.

Funding Coordenação de Aperfeiçoamento de Pessoal de Nível Superior.

References

1. Sehitoglu H (1996) Thermal and thermomechanical fatigue of structural alloys. In: Sehitoglu H (ed) ASM handbook-fatigue and fracture, vol 9. ASM International, Ohio, pp 527–556
2. Srinivasan VS, Valsan M, Rao BS, Mannan SL, Raj B (2003) Low cycle fatigue and creep-fatigue interaction behavior of 316L(N) stainless and life prediction by artificial neural network approach. Int J Fatigue 25:1327–1338. https://doi.org/10.1016/S0142-1123(03)00064-1
3. González R, González A, Talamantes-Silva J, Valtierra S, Mercado-Solís RD, Garza-Montes-de-Oca NF, Colás R (2013) Fatigue of an aluminum cast alloy used in manufacturing automotive engine blocks. Int J Fatigue 54:118–126. https://doi.org/10.1016/j.ijfatigue.2013.03.018
4. Koutiri I, Bellett D, Morel F, Augustins L, Adrien J (2013) High cycle fatigue damage mechanisms in cast aluminum subject to complex loads. Int J Fatigue 47:44–57. https://doi.org/10.1016/j.ijfatigue.2012.07.008
5. Cai C, Liaw PK, Ye M, Yu J (1999) Recent developments in the thermomechanical fatigue life prediction of superalloys. J Mater 51(4):1–19
6. Sarabanda JVL (1991) Estudo de fadiga sob controle de deformação de duas ligas de alumínio empregadas em pistões de motores diesel. Dissertação de Mestrado, Escola Politécnica—USP, São Paulo. https://doi.org/10.11606/D.3.1993.tde-16082024-112517.
7. Odegard JA, Pedersen K (1994) Fatigue properties of an A356 (AlSi7Mg) aluminum alloy for automotive applications-fatigue life prediction. SAE technical paper, Society of Automotive Engineers, Warrendale PA, Report SAE-940811, p. 25–32. https://doi.org/10.4271/940811.
8. Buffière JY, Savelli S, Jouneau PH, Maire E, Fougères R (2001) Experimental study of porosity and its relation to fatigue mechanisms of model Al-Si7-Mg0.3 cast Al alloys. Mater Sci Eng A 316:115–126. https://doi.org/10.1016/S0921-5093(01)01225-4
9. Meyer-Olbersleben F, Engler-Pinto CC, RézaÏ-Aria F (1996) On thermal fatigue of nickel-based superalloys. In: Verrilli MJ, Castelli MG (eds) Thermomechanical fatigue behavior of materials: second volume. ASTM International, West Conshohocken, pp 41–55. https://doi.org/10.1520/STP16445S
10. Pommier S, Bompard P (2000) Bauschinger effect of alloys and plasticity-induced crack closure: a finite element analysis. Fat Fract of Engng Mater Struct 23(2):129–139. https://doi.org/10.1046/j.1460-2695.2000.00259.x
11. Pommier S, Risbet M (2005) Time derivative equations for fatigue crack growth in metals. Int Jal of Fracture 131(1):79–106. https://doi.org/10.1016/j.ijfatigue.2005.06.034
12. Pommier S, Hamam R (2007) Incremental model for fatigue crack growth based on a displacement partitioning hypothesis of mode I elastic-plastic displacement fields. Fatigue Fract Eng Mater Struct 30:582–598. https://doi.org/10.1111/j.1460-2695.2007.01128.x
13. ASTM B108/B108M-12e1 (2012) Standard Specification for Aluminum-Alloy Permanent Mold Castings. ICS Number Code 77.150.10 (Aluminium products), UNSPSC Code 31121300 (Machined permanent mold castings); 31101706 (Aluminum permanent mold casting), https://doi.org/10.1520/B0108_B0108M-12E01.
14. Cheremisinoff NP (1996) Materials selection deskbook. Westwood, New Jersey, pp 86–93
15. ASM Metals Handbook (1990) Properties and Selection Nonferrous Alloys and Special-Purpose Materials, v. 2, p. 484–666. https://doi.org/10.31399/asm.hb.v02.9781627081627.
16. ASTM E3-11 (2011) Standard Guide for Preparation of Metallographic Specimens. ICS Number Code 77.040.99 (Other methods of testing metals), UNSPSC Code 41111720 (Scanning electron microscopes), https://doi.org/10.1520/E0003-11.
17. ASM Metals Handbook (2004) Metallography and Microstructures. v. 9, In: George F (ed) Vander Voort. ISBN: 978-0-87170-706-2.
18. ASTM E21-09 (2009) Standard Test Methods for Elevated Temperature Tension Tests of Metallic Materials. ICS Number Code 77.040.10 (Mechanical testing of metals), https://doi.org/10.1520/E0021-09.
19. ASTM E8/E8M-13a (2013) Standard Test Methods for Tension Testing of Metallic Materials. ICS Number Code 77.040.10 (Mechanical testing of metals), UNSPSC Code 41114621(Tension testers), https://doi.org/10.1520/E0008_E0008M.
20. ASTM E606/E606M-12 (2012) Standard Test Method for Strain-Controlled Fatigue Testing. ICS Number Code 77.040.10 (Mechanical testing of metals), UNSPSC Code 41114608(Fatigue testers), https://doi.org/10.1520/E0606_E0606M-12.
21. ASTM E2368-10 (2010) Standard Practice for Strain Controlled Thermomechanical Fatigue Testing. ICS Number Code 19.060

(Mechanical testing), UNSPSC Code 41114608 (Fatigue testers), https://doi.org/10.1520/E2368-10.
22. Pickard AC (1986) The application of 3-dimensional finite element methods to fracture mechanics and fatigue life prediction. Engineering Materials Advisory Services Ltd EMAS, West Midlands, UK, p 550
23. ASTM A356/A356M-11 (2011) Standard Specification for Steel Castings, Carbon, Low Alloy, and Stainless Steel, Heavy-Walled for Steam Turbines. ICS Number Code 77.140.80 (Iron and steel castings), UNSPSC Code 31101603(Steel sand casting), 31101604(Stainless steel sand casting), https://doi.org/10.1520/A0356_A0356M-11.
24. Crepeau PN (1998) The effects of addition of iron in aluminum-silicon alloys. Casting and Services, v.5, p. 68, Cooperative Research Centre for Cast Metals Manufacturing (CAST). The University of Queensland Brisbane, Australia.
25. Suresh S (1998) Fatigue of materials. Cambridge University Press, Cambridge, UKS
26. ASTM E1457-13 (2013) Standard Test Method for Measurement of Creep Crack Growth Times and Rates in Metals. ICS Number Code 77.040.10 (Mechanical testing of metals), UNSPSC Code 41114606 (Creep testers), https://doi.org/10.1520/E1457-13.
27. Roesler J, Harders H, Baeker M (2007) Mechanical behavior of engineering materials, metals, ceramics, polymers, and composites. Springer, Berlin Heidelberg, New York, p 536
28. Kruch S, Chaboche J-L, Prigent S (1995) A fracture mechanics-based fatigue-creep-environment crack growth model at high temperatures. Int J Press Vess Pipping 59:141–148. https://doi.org/10.1016/0308-0161(94)90149-X
29. Lemaitre J, Chaboche J-L, et al (2020) Mécanique des matériaux solides. Paris. Parution: février 2020, Collection: Sciences Sup, Marque: Dunod. ISBN 2100541331, 9782100541331.